Interpreting the 95 GeV di-photon and di-tau excesses in the Georgi–Machacek model*

Qin Chang (常钦)[1,2,3†] Xiaokang Du (都小康)[1,2‡] Pengxuan Zhu (朱鹏轩)[4§]

[1]Institute of Physics, Henan Academy of Sciences, Zhengzhou 450046, China
[2]Centre for Theoretical Physics, Henan Normal University, Xinxiang 453007, China
[3]Center for High Energy Physics, Henan Academy of Sciences, Zhengzhou 455004, China
[4]ARC Centre of Excellence for Dark Matter Particle Physics & CSSM, Department of Physics, Adelaide University, Adelaide, SA 5005, Australia

Abstract: We revisit the 95 GeV $\gamma\gamma$ and $\tau\tau$ excesses in the Georgi–Machacek model using a combined fit to a single light CP-even custodial singlet H. By combining the one-loop renormalization group-improved effective potential and positive-definiteness conditions for vacuum stability with perturbative unitarity, electroweak precision tests, B-physics, and Higgs data, we identify a narrow but viable parameter region. In the allowed region, $\mu_{\gamma\gamma}$ approaches the experimental central value, whereas $\mu_{\tau\tau}$ reaches only ~ 0.5 (about 1.4σ below the CMS central value) and remains within the 2σ interval—providing a good description of the di-photon excess but only a partial accommodation of the di-tau excess. The scenario predicts characteristic patterns in the singlet mixing and triplet vacuum expectation values and is highly testable at the HL-LHC and future lepton colliders through precision κ_V measurements and direct exotic searches.

Keywords: the Georgi–Machacek model, the positive-definiteness condition, the 95 GeV excesses

DOI: 10.1088/1674-1137/ae9f36 **CSTR:** 32044.14.ChinesePhysicsC.51013103

I. INTRODUCTION

The discovery of the 125 GeV Higgs boson by the ATLAS [1] and CMS [2] Collaborations in 2012 confirmed the Standard Model (SM) framework of electroweak symmetry breaking (EWSB). Nevertheless, theoretical motivations and the sizable uncertainties in current Higgs data fits still leave ample room for an extended Higgs sector [3]. Consequently, the search for additional scalar fields remains a crucial objective.

The CMS and ATLAS Collaborations have each reported a di-photon excess around 95.4 GeV [4−6]. A phenomenological combination of these Run-2 di-photon results in [7] finds a local significance of 3.1σ and a combined signal strength $\mu_{\gamma\gamma}^{\rm ATLAS+CMS} = 0.24^{+0.09}_{-0.08}$. CMS has also observed another scalar resonance at 100 GeV with a local significance of 3.1σ [8]. Because the mass resolution in the di-tau channel is poorer than in the di-photon channel, this excess could be compatible with the same scalar as the di-photon excess. At 95 GeV, the local significance in the di-tau channel is 2.6σ, with a signal strength of $\mu_{\tau\tau}^{\rm CMS} = 1.2 \pm 0.5$. Additionally, data from the Large Electron-Positron Collider (LEP) show an excess at 98 GeV in the $b\bar{b}$ channel, with a local significance of 2.3σ and a signal strength of $\mu_{b\bar{b}}^{\rm LEP} = 0.117 \pm 0.057$ [9].

Although each excess is individually modest in significance, their persistence motivates a systematic exploration within well-defined new physics frameworks. Since the three excesses cluster in a similar mass region and exhibit signal strengths comparable to those expected from a SM-like Higgs boson, it is natural to view them as potential hints of an extended Higgs sector in the context of EWSB. It is therefore important to examine whether they can be consistently interpreted as manifestations of a light

Received 23 June 2026; Accepted 25 August 2026; Accepted manuscript online 26 August 2026

* Supported by the National Natural Science Foundation of China (12447167, 12275067), the Joint Fund of Henan Province Science and Technology R&D Program (225200810030, 225200810092 and 225200810014), the Startup Research Fund of Henan Academy of Sciences (231820011), the Basic Research Fund of Henan Academy of Sciences (240620006), the Graduate Innovation Fund of Henan Academy of Sciences (243320031), the National Key R&D Program of China (2023YFA1606000) and the Science and Technology Innovation Leading Talent Support Program of Henan Province (254000510039). PZ is supported by the ARC Discovery Project DP220100007 and the Centre for the Subatomic Structure of Matter (CSSM)

† E-mail: changqin@htu.edu.cn
‡ E-mail: xkdu@hnas.ac.cn (Corresponding author)
§ E-mail: pengxuan.zhu@adelaide.edu.au

Content from this work may be used under the terms of the Creative Commons Attribution 3.0 licence. Any further distribution of this work must maintain attribution to the author(s) and the title of the work, journal citation and DOI. Article funded by SCOAP[3] and published under licence by Chinese Physical Society and the Institute of High Energy Physics of the Chinese Academy of Sciences and the Institute of Modern Physics of the Chinese Academy of Sciences and IOP Publishing Ltd

scalar particle. There is broad theoretical interest in simultaneously explaining the di-photon, di-tau, and $b\bar{b}$ excesses within a consistent framework. [7, 10, 11] These include scalar extensions [12, 13], dilaton models [14, 15], extra-U(1) symmetry [16–20], left-right models [21], triplet Higgs models [22], scotogenic models [23–25], Higgs radion models [26, 27], and other mechanisms [28–30]. Discussions have also been carried out in various versions of the two-Higgs-doublet model (2HDM) [31–44], and in the singlet-extended 2HDM [45–56]. In a supersymmetric framework, the minimal supersymmetric standard model (MSSM) cannot provide a common explanation [57]. By contrast, a well-motivated supersymmetric explanation of the observed excesses is provided by the next-to-minimal supersymmetric standard model (NMSSM), in which a mostly singlet-like Higgs boson can naturally appear around 95 GeV [58–68]. Another concrete example is provided by the $\mu\nu$SSM, where the CP-even right-handed sneutrino may play the role of a light scalar explaining the excesses [69, 70]. Beyond these cases, further supersymmetric scenarios, such as the minimal R-symmetry supersymmetric standard model (MRSSM) [71, 72], have also been explored as possible solutions accommodating a light scalar state. Finally, several works have approached the problem from a collider perspective [73–79].

The Georgi-Machacek (GM) model [80–91] extends the SM by introducing a complex $SU(2)_L$ triplet scalar χ with hypercharge +1 and a real $SU(2)_L$ triplet scalar ξ with hypercharge 0. The field content is arranged such that custodial symmetry is preserved at tree level after EWSB, provided the triplet vacuum expectation values (VEVs) are aligned, $v_\chi = v_\xi \equiv v_\Delta$. This alignment permits v_Δ values up to several tens GeV, significantly larger than in generic triplet extensions, while maintaining $\rho_{\text{tree}} = 1$. The model predicts nine additional scalar states, including a characteristic doubly charged Higgs boson, resulting in a rich phenomenology and distinctive collider signatures [92–124]. Notably, the GM model allows the couplings of the SM-like Higgs boson to weak gauge bosons to exceed their SM values [125–127].

The extended scalar sector improves vacuum stability and can induce a strong first-order electroweak phase transition (EWPT), potentially generating gravitational-wave signals accessible to future experiments [128–132]. If lepton number violation is present, triplet-lepton interactions can generate neutrino masses [133–136]. The GM framework has also been employed to address the W-mass anomaly reported by CDF-II [136–139], especially when custodial symmetry-breaking effects are included [140–142]. Furthermore, the light custodial singlet scalar of the GM model constitutes a natural candidate to interpret the excesses observed near 95 GeV [143–147]. An explanation for the excesses observed in the $\gamma\gamma$, $\tau\tau$, and $b\bar{b}$ channels requires a near-degenerate CP-even/CP-odd 'twin-peak' structure [143]; with only a single light CP-even state, the $\tau\tau$ excess is in tension with the $\gamma\gamma$ and $b\bar{b}$ channels [143–145]. Recent analyses, however, strongly disfavor the LEP $b\bar{b}$ excess as evidence for a new scalar [78], motivating a focus on the LHC-driven $\gamma\gamma$ and $\tau\tau$ channels.

The positive-definiteness vacuum stability conditions for the GM model were proposed in [148], which preclude the existence of deeper vacua in large-field regions. Moving beyond the conventional tree-level analysis, the study employs the one-loop renormalization group-improved (RG-improved) effective potential, along with a novel criterion for the positive definiteness of homogeneous polynomials in multiple variables—a refinement necessitated by loop-induced custodial symmetry-breaking effects. Through numerical analysis, it is shown that the quartic coupling ranges permitted by the positive-definiteness requirements significantly deviate from those derived from tree-level bounded-from-below conditions. Notably, certain parameter regions previously excluded by tree-level criteria become viable when the one-loop RG-improved scalar potential is considered. Conversely, some regions of parameter space that satisfy tree-level bounded-from-below constraints at the electroweak scale are ultimately ruled out by the positive-definiteness requirements of the effective potential in large-field regions.

The distinctive aim of this work is to quantify how the one-loop RG-improved positive-definiteness condition affects a single light CP-even scalar interpretation of the LHC $\gamma\gamma$ and $\tau\tau$ indications. Relative to Ref. [144] (tree-level BFB), the viable di-tau strength is enlarged from $O(0.1)$ to ~ 0.5; relative to Ref. [145], the LEP $b\bar{b}$ excess is not used as a fitting input; and unlike Ref. [143], we retain one light CP-even scalar rather than a twin-peak construction. The CMS di-tau central value remains inaccessible because of tension with the 125 GeV Higgs couplings.

This work is organized as follows. In Sec. II, we provide a brief review of the GM model. A short discussion of the di-photon and di-tau excess signals around 95 GeV is presented in Sec. III. Theoretical and experimental constraints relevant to realistic studies within the GM model are detailed in Sec. IV. Numerical results are displayed in Sec. V. Finally, we present our conclusions in Sec. VI.

II. THE GEORGI-MACHACEK MODEL

The GM model augments the SM scalar sector by introducing additional triplet fields. It contains the familiar $SU(2)_L$ doublet (ϕ^+, ϕ^0) with hypercharge 1/2, a complex triplet $(\chi^{++}, \chi^+, \chi^0)$ with hypercharge +1, and a real triplet $(\xi^+, \xi^0, -\xi^{+*})$ with zero hypercharge. This field content allows custodial $SU(2)_V$ symmetry at tree level

and leads to distinctive scalar phenomenology.

To clarify custodial symmetry, the doublet and triplets are arranged into the matrices Φ and Δ, respectively:

$$\Phi = \begin{pmatrix} \phi^{0*} & \phi^{+} \\ \phi^{-} & \phi^{0} \end{pmatrix}, \quad \Delta = \begin{pmatrix} \chi^{0*} & \xi^{+} & \chi^{++} \\ \chi^{-} & \xi^{0} & \chi^{+} \\ \chi^{-} & \xi^{-} & \chi^{0} \end{pmatrix}. \tag{1}$$

The most general scalar potential for the GM scalar sector, constructed to be invariant under a global $SU(2)_L \times SU(2)_R$ symmetry and, consequently, also under its gauged subgroup $SU(2)_L \times U(1)_Y$, reads

$$\begin{aligned} V(\Phi,\Delta) =& \frac{1}{2}m_\Phi^2 \mathrm{tr}\left[\Phi^\dagger\Phi\right] + \frac{1}{2}m_\Delta^2 \mathrm{tr}\left[\Delta^\dagger\Delta\right] + \lambda_1\left(\mathrm{tr}\left[\Phi^\dagger\Phi\right]\right)^2 \\ &+ \lambda_2\left(\mathrm{tr}\left[\Delta^\dagger\Delta\right]\right)^2 + \lambda_3 \mathrm{tr}\left[\left(\Delta^\dagger\Delta\right)^2\right] \\ &+ \lambda_4 \mathrm{tr}\left[\Phi^\dagger\Phi\right]\mathrm{tr}\left[\Delta^\dagger\Delta\right] \\ &+ \lambda_5 \mathrm{tr}\left[\Phi^\dagger\frac{\sigma^a}{2}\Phi\frac{\sigma^b}{2}\right]\mathrm{tr}\left[\Delta^\dagger T^a \Delta T^b\right] \\ &+ \mu_1 \mathrm{tr}\left[\Phi^\dagger\frac{\sigma^a}{2}\Phi\frac{\sigma^b}{2}\right](P^\dagger\Delta P)_{ab} \\ &+ \mu_2 \mathrm{tr}\left[\Delta^\dagger T^a \Delta T^b\right](P^\dagger\Delta P)_{ab}, \end{aligned} \tag{2}$$

Here, σ^i denote the Pauli matrices, and T^i denote the $SU(2)$ generators in the triplet representation:

$$T^1 = \frac{1}{\sqrt{2}}\begin{pmatrix} 0 & 1 & 0 \\ 1 & 0 & 1 \\ 0 & 1 & 0 \end{pmatrix}, \quad T^2 = \frac{1}{\sqrt{2}}\begin{pmatrix} 0 & -\mathrm{i} & 0 \\ \mathrm{i} & 0 & -\mathrm{i} \\ 0 & \mathrm{i} & 0 \end{pmatrix},$$
$$T^3 = \begin{pmatrix} 1 & 0 & 0 \\ 0 & 0 & 0 \\ 0 & 0 & -1 \end{pmatrix}. \tag{3}$$

The P matrix rotates the triplet fields Δ into the Cartesian basis

$$P = \frac{1}{\sqrt{2}}\begin{pmatrix} -1 & \mathrm{i} & 0 \\ 0 & 0 & \sqrt{2} \\ 1 & \mathrm{i} & 0 \end{pmatrix}. \tag{4}$$

Note that the last two terms in Eq. (2) vanish under a $\mathbb{Z}_2$ symmetry. However, we retain them in this work.

Under $SU(2)_L \times SU(2)_R$, the fields Φ and Δ transform as

$$\Phi \to U_L \Phi U_R^\dagger, \quad \Delta \to U_L \Delta U_R^\dagger. \tag{5}$$

Here, $U_{L,R}$ denotes $\exp(\mathrm{i}\theta_{L,R}^a \sigma^a)$ for the doublet and $\exp(\mathrm{i}\theta_{L,R}^a T^a)$ for the triplet. The SM electroweak gauge group $SU(2)_L \times U(1)_Y$ is embedded in the global $SU(2)_L \times SU(2)_R$ symmetry, where $SU(2)_L$ is identified with the generators T_L^i and the hypercharge $U(1)_Y$ is associated with the generator T_R^3.

After EWSB, the neutral scalar fields can be parameterized as

$$\begin{aligned} &\xi^0 \to v_\xi + h_\xi, \\ &\phi^0 \to \frac{1}{\sqrt{2}}\left(v_\phi + h_\phi + \mathrm{i}a_\phi\right) \\ &\chi^0 \to v_\chi + \frac{1}{\sqrt{2}}\left(h_\chi + \mathrm{i}a_\chi\right). \end{aligned} \tag{6}$$

Here, the parameters v_ξ, v_ϕ, and v_χ denote the VEVs of the corresponding neutral components of these scalar fields. Then, the tree-level ρ parameter of the GM model can be expressed as

$$\rho_{\mathrm{tree}} \equiv \frac{m_W^2}{m_Z^2 \cos^2\theta_W} = \frac{v_\phi^2 + 4v_\chi^2 + 4v_\xi^2}{v_\phi^2 + 8v_\chi^2}. \tag{7}$$

Therefore, when the triplet VEVs are aligned, $v_\chi = v_\xi \equiv v_\Delta$, the vacuum is invariant only under the diagonal (custodial) subgroup $SU(2)_V \subset SU(2)_L \times SU(2)_R$ (*i.e.*, when $U_L = U_R$). Consequently, the tree-level ρ parameter automatically satisfies $\rho_{\mathrm{tree}} = 1$. In this alignment limit, the VEVs of the scalar fields take the form

$$\langle\Phi\rangle = \frac{v_\phi}{\sqrt{2}}\mathbf{I}_{2\times2}, \quad \text{and} \quad \langle\Delta\rangle = v_\Delta \mathbf{I}_{3\times3}. \tag{8}$$

The condition for EWSB is given by

$$v^2 = v_\phi^2 + 8v_\Delta^2 \simeq (246\ \mathrm{GeV})^2. \tag{9}$$

The physical scalars are then decomposed into irreducible representations under the custodial $SU(2)_V$ symmetry. The doublet Φ (interpreted as a $\mathbf{2}\otimes\mathbf{2}$ representation) decomposes into $\mathbf{1}\oplus\mathbf{3}$, whereas the triplet Δ (as a $\mathbf{3}\otimes\mathbf{3}$ representation) decomposes into $\mathbf{1}\oplus\mathbf{3}\oplus\mathbf{5}$. One triplet, G_3, provides the Nambu-Goldstone bosons eaten by the W and Z bosons

$$\begin{aligned} G_3^\pm &= \cos\theta_H \phi^\pm + \frac{\sin\theta_H}{\sqrt{2}}\left(\chi^\pm + \xi^\pm\right), \\ G_3^0 &= \cos\theta_H a_\phi + \sin\theta_H a_\chi, \end{aligned} \tag{10}$$

where the mixing parameter θ_H is defined as

$$\tan\theta_H \equiv 2\sqrt{2}v_\Delta/v_\phi. \tag{11}$$

The singlet H_1^0 (originating from the Δ field), the triplet ($H_3^\pm$ and H_3^0), and the quintuplet ($H_5^{\pm\pm}$, $H_5^\pm$, and H_5^0) are given by

$$\begin{aligned}
H_1^0 &= \sqrt{\frac{2}{3}}h_\chi + \sqrt{\frac{1}{3}}h_\xi,\\
H_3^\pm &= -\sin\theta_H\phi^\pm + \frac{\cos\theta_H}{\sqrt{2}}\left(\chi^\pm + \xi^\pm\right),\\
H_3^0 &= \cos\theta_H a_\chi - \sin\theta_H a_\phi,\\
H_5^{\pm\pm} &= \chi^{\pm\pm}, \quad H_5^\pm = \frac{1}{\sqrt{2}}\left(\chi^\pm - \xi^\pm\right),\\
H_5^0 &= \sqrt{\frac{2}{3}}h_\xi - \sqrt{\frac{1}{3}}h_\chi.
\end{aligned} \tag{12}$$

In the basis (h_ϕ, H_1^0, H_5^0), the mass matrix for the CP-even Higgs states is given by

$$M^2_{\text{CP-even}} = \begin{pmatrix} M_{11}^2 & M_{12}^2 & 0\\ M_{12}^2 & M_{22}^2 & 0\\ 0 & 0 & m_{H_5}^2 \end{pmatrix}, \tag{13}$$

where the elements of the 2×2 block are

$$\begin{aligned}
M_{11}^2 &= 8\lambda_1 v_\phi^2,\\
M_{12}^2 &= M_{21}^2 = \frac{\sqrt{3}}{2}v_\phi\left(4\left(2\lambda_4+\lambda_5\right)v_\Delta + \mu_1\right),\\
M_{22}^2 &= 8\left(\lambda_3+3\lambda_2\right)v_\Delta^2 - \frac{v_\phi^2}{4v_\Delta}\mu_1 + 6v_\Delta\mu_2.
\end{aligned} \tag{14}$$

The mass eigenstates h and H are defined by

$$h = \cos\alpha h_\phi - \sin\alpha H_1^0, \quad H = \sin\alpha h_\phi + \cos\alpha H_1^0, \tag{15}$$

where the mixing angle α is defined by

$$\tan2\alpha = \frac{2M_{12}^2}{M_{22}^2 - M_{11}^2}, \quad \alpha\in(-\pi/2,\pi/2). \tag{16}$$

The masses of all Higgs mass eigenstates can then be expressed as

$$\begin{aligned}
m_h^2 &= M_{11}^2\cos^2\alpha + M_{22}^2\sin^2\alpha + M_{12}^2\sin2\alpha,\\
m_H^2 &= M_{11}^2\sin^2\alpha + M_{22}^2\cos^2\alpha - M_{12}^2\sin2\alpha,\\
m_{H_3}^2 &\equiv m_{H_3^\pm}^2 = m_{H_3^0}^2 = -\frac{v^2}{4v_\Delta}\mu_1 - \frac{1}{2}\lambda_5 v^2,\\
m_{H_5}^2 &\equiv m_{H_5^{\pm\pm}}^2 = m_{H_5^\pm}^2 = m_{H_5^0}^2 = -\frac{v_\phi^2}{4v_\Delta}\mu_1 - 12v_\Delta\mu_2\\
&\quad + 8\lambda_3 v_\Delta^2 - \frac{3}{2}\lambda_5 v_\phi^2.
\end{aligned} \tag{17}$$

By applying the tadpole conditions

$$\left.\frac{\partial V}{\partial h_\phi}\right|_0 = 0, \quad \left.\frac{\partial V}{\partial h_\xi}\right|_0 = 0, \quad \left.\frac{\partial V}{\partial h_\chi}\right|_0 = 0. \tag{18}$$

The mass parameters m_ϕ^2 and m_Δ^2 in Eq. (2) can be eliminated as follows:

$$\begin{aligned}
m_\phi^2 &= -4\lambda_1 v_\phi^2 - \left(\frac{3\mu_1}{2v_\Delta} + 6\lambda_4 + 3\lambda_5\right)v_\Delta^2,\\
m_\Delta^2 &= -\left(12\lambda_2 + 4\lambda_3\right)v_\Delta^2 - \left(\frac{1}{4v_\Delta}\mu_1 + 2\lambda_4 + \lambda_5\right)v_\phi^2 - 6v_\Delta\mu_2.
\end{aligned} \tag{19}$$

In summary, the free parameters of the GM model consist of five dimensionless couplings $\lambda_{1,2,3,4,5}$, two dimensional parameters $\mu_{1,2}$, and one mixing parameter θ_H. In this work, we adopt the following set of free parameters in practice:

$$\lambda_{2,3,4,5}, \quad m_h^{\text{In}}, \quad m_H^{\text{In}}, \quad \alpha, \quad \sin\theta_H, \tag{20}$$

where $\mu_{1,2}$ are replaced by $m_{h,H}^{\text{In}}$, and λ_1 is replaced by α. In the following sections, $m_{h,H}$ without a superscript denotes the physical pole mass as calculated by the spectrum calculator.

III. 95 GEV EXCESSES IN THE GM MODEL

In the setup introduced in Sec. II, the GM model contains two light singlet scalar fields. In this work, the heavier state, denoted by h, is identified with the 125 GeV SM-like Higgs boson. The other state, denoted by H, serves as a candidate to explain the observed excesses around 95 GeV. The couplings of these Higgs states to SM fermions (f) and weak gauge bosons ($V = W,Z$) are modified as follows:

$$\begin{aligned}
g_{hff} &= \kappa_F \times g_{hff}^{\text{SM}}, \quad g_{hVV} = \kappa_V \times g_{hVV}^{\text{SM}},\\
g_{Hff} &= \kappa_F^H \times g_{hff}^{\text{SM}}, \quad g_{HVV} = \kappa_V^H \times g_{hVV}^{\text{SM}},
\end{aligned} \tag{21}$$

with the effective Higgs couplings κ at leading order

$$\kappa_F = \frac{\cos\alpha}{\cos\theta_H}, \quad \kappa_V = \cos\theta_H\cos\alpha - \sqrt{\frac{8}{3}}\sin\theta_H\sin\alpha,$$

$$\kappa_F^H = \frac{\sin\alpha}{\cos\theta_H}, \quad \kappa_V^H = \cos\theta_H\sin\alpha + \sqrt{\frac{8}{3}}\sin\theta_H\cos\alpha. \tag{22}$$

Using this framework, the GM predictions for the di-photon signal strength normalized to the SM prediction, $\mu_{\gamma\gamma}$, are given by

$$\mu_{\gamma\gamma} \equiv \frac{\sigma_{\rm GM}(pp\to H_{95}\to\gamma\gamma)}{\sigma_{\rm SM}(pp\to h_{95}\to\gamma\gamma)} \simeq \frac{\sigma_{\rm GM}(gg\to H_{95})}{\sigma_{\rm SM}(gg\to h_{95})} \times \frac{\mathcal{B}_{\rm GM}(H_{95}\to\gamma\gamma)}{\mathcal{B}_{\rm SM}(h_{95}\to\gamma\gamma)} = \left|\kappa_F^H\right|^2 \times \frac{\mathcal{B}_{\rm GM}(H_{95}\to\gamma\gamma)}{1.39\times10^{-3}}, \tag{23}$$

where the Higgs-boson mass is fixed at approximately 95 GeV (denoted by H_{95} and h_{95}), and the subscript GM (SM) denotes the GM (SM) prediction for the inclusive production rate of H_{95} (h_{95}). The specific value 1.39×10^{-3} is the SM Higgs branching ratio at 95 GeV, as calculated by the LHC Higgs Cross Section Working Group [149]. The approximation in the second line arises because SM Higgs production is dominated by the gluon-gluon fusion process, which accounts for approximately 89% of the total Higgs production at a mass of 95 GeV [149]. The third line follows because the gluon-gluon fusion process ($gg\to h$) is mediated by a colored-fermion loop. As a result, the effective coupling κ_{gg}^H equals κ_F^H, since the fermionic couplings of H scale universally as κ_F^H at leading order, as shown in Eq. (22). Similarly, the GM predictions for the signal strengths in the $\tau\tau$ and bb channels are given by

$$\mu_{bb} \equiv \frac{\sigma_{\rm GM}(e^+e^-\to ZH_{95}(H_{95}\to bb))}{\sigma_{\rm SM}(e^+e^-\to Zh_{95}(h_{95}\to bb))} = \left|\kappa_V^H\right|^2 \times \frac{\mathcal{B}_{\rm GM}(H_{95}\to bb)}{0.801},$$

$$\mu_{\tau\tau} \equiv \frac{\sigma_{\rm GM}(pp\to H_{95}\to\tau\tau)}{\sigma_{\rm SM}(pp\to h_{95}\to\tau\tau)} \simeq \left|\kappa_F^H\right|^2 \times \frac{\mathcal{B}_{\rm GM}(H_{95}\to\tau\tau)}{8.32\times10^{-2}}. \tag{24}$$

From the above definitions, all signal strengths are expressed in terms of the ratio $\sigma_{\rm GM}/\sigma_{\rm SM}$, so QCD corrections to the numerator and denominator largely cancel. This reduces the theoretical uncertainty in the predicted signal strengths. The LEP $b\bar{b}$ relation is exact at leading order (Higgsstrahlung $\propto|\kappa_V^H|^2$). The inclusive LHC $\tau\tau$ relation is approximate: it assumes gluon-fusion dominance and neglects smaller κ_V^H-dependent production modes.

We now examine the branching ratios. The partial decay width of the lighter scalar H into SM final states can be expressed as

$$\Gamma(H\to XX) = |\kappa_X^H|^2 \times \Gamma_{\rm SM}(h\to XX)\big|_{m_h=m_H}, \tag{25}$$

where $\Gamma_{\rm SM}(h\to XX)\big|_{m_h=m_H}$ is the SM Higgs partial decay width evaluated at the mass m_H. Therefore, the total decay width of the custodial-singlet state H can be written as

$$\Gamma_H^{\rm tot} = \Gamma_h^{\rm SM}\sum_X \left|\kappa_X^H\right|^2 \mathcal{B}_{\rm SM}(h\to XX), \tag{26}$$

where the SM Higgs total decay width $\Gamma_h^{\rm SM}$ and branching ratios $\mathcal{B}_{\rm SM}(h\to XX)$ are evaluated at m_H. The couplings of the neutral scalars H and h to photons are induced by charged-particle loops. In the SM, Higgs-boson decay into two photons is mediated by W-boson and heavy charged-fermion loops, dominated by the top quark. In the GM model, loops of heavy charged Higgs states S_i (including $H_5^{\pm\pm}$, $H_5^{\pm}$, and $H_3^{\pm}$) can significantly enhance the partial decay width $\Gamma(H\to\gamma\gamma)$. The corresponding effective coupling $\kappa_{\gamma\gamma}^H$ can be expressed as

$$\kappa_\gamma^H = \frac{\sum_i \frac{g_{HS_iS_i}}{2m_{S_i}^2} vQ_{S_i}^2 A_0\left(\frac{m_H^2}{4m_{S_i}^2}\right) + \kappa_V^H A_1\left(\frac{m_H^2}{4m_W^2}\right) + \kappa_F^H \frac{4}{3}A_{1/2}\left(\frac{m_H^2}{4m_t^2}\right)}{A_1\left(\frac{m_H^2}{4m_W^2}\right) + \frac{4}{3}A_{1/2}\left(\frac{m_H^2}{4m_t^2}\right)}, \tag{27}$$

where $g_{HS_iS_i}$ are the scalar trilinear couplings of H to the charged states S_i, and the loop functions $A_{0,1/2,1}$ can be found in the literature [84, 150, 151]. For an H boson with mass 95 GeV, $A_1\simeq-7.6$ and $A_{1/2}\approx4/3$. The factor A_0 reaches its maximum value of $1.5+\mathrm{i}$ at $m_H=2m_{S_i}$, while in the limit of very heavy loop charged scalars, $A_0(0)\simeq1/3$.

Then, the signal strength in Eq. (23) and Eq. (24) can be rewritten as:

$$\mu_{\gamma\gamma} = \left|\kappa_F^H\right|^2\left|\kappa_\gamma^H\right|^2\cdot\frac{\Gamma_h^{\rm SM}}{\Gamma_H^{\rm tot}},$$
$$\mu_{bb} = \left|\kappa_V^H\right|^2\left|\kappa_F^H\right|^2\cdot\frac{\Gamma_h^{\rm SM}}{\Gamma_H^{\rm tot}},$$
$$\mu_{\tau\tau} = \left|\kappa_F^H\right|^4\cdot\frac{\Gamma_h^{\rm SM}}{\Gamma_H^{\rm tot}}. \tag{28}$$

It is clear that all three signal strengths share a common factor, $\left|\kappa_F^H\right|^2\cdot\frac{\Gamma_h^{\rm SM}}{\Gamma_H^{\rm tot}}$. This creates tension in attributing all observed excesses to a single source. Charged scalar

states in the GM model can provide positive contributions to the $\gamma\gamma$ excess, especially the doubly charged $H_5^{\pm\pm}$ with $Q_S^2 = 4$. Ref. [144] investigates various possibilities for H to explain the $\gamma\gamma$, $\gamma\gamma + bb$, and $\gamma\gamma + bb + \tau\tau$ excesses. However, recent dedicated reanalyses argue that this feature is unlikely to arise from a genuine new scalar resonance [78]. Given the limited di-jet mass resolution at LEP and these updated conclusions, we do not attempt to accommodate the $b\bar{b}$ hint in this work. Instead, we focus on the two LHC-driven channels ($\gamma\gamma$ and $\tau\tau$), where the experimental systematics and resolutions are better controlled in the relevant mass window. Finally, we note that all loop-induced rates, branching ratios, and total widths in our scan are evaluated with the spectrum tools described in Sec. IV.

IV. METHODOLOGY AND CONSTRAINTS

To realize a light custodial-singlet scalar H near 95.4 GeV that can accommodate the LHC hints in the $\gamma\gamma$ and $\tau\tau$ channels, we perform a comprehensive parameter scan. This section describes the scan methodology together with the various constraints imposed. The detailed numerical results corresponding to these constraints will be presented in Sec. V.

In practice, we use the package `GMCALC` [152], a dedicated calculator for the GM model. Alternatively, we use the `SPheno` package [153, 154] in combination with `SARAH` [155–159] to compute the GM model spectrum.

We carry out a comprehensive parameter scan using the JARVIS-HEP framework [160]. The input parameters in Eq. (20) are scanned over the following ranges:

$$\begin{aligned} &-\sqrt{4\pi} < \lambda_{2,3,4,5} < \sqrt{4\pi}, \quad 120\ \text{GeV} < m_h^{\text{In}} < 130\ \text{GeV}, \\ &90\ \text{GeV} < m_H^{\text{In}} < 102\ \text{GeV}, \\ &0 < \sin\theta_H < 0.4, \quad \pi/4 < |\alpha| < \pi/2. \end{aligned} \tag{29}$$

To assess the overall viability of the GM model in explaining the observed excesses, we construct a likelihood-based framework. The total likelihood $\mathcal{L}_{\text{tot}}$ is defined as

$$\begin{aligned} \mathcal{L}_{\text{tot}} &= \exp\left(-\frac{1}{2}\chi^2_{\text{tot}}\right) \times \Theta_{\text{PD}}\Theta_{\text{unit}}\Theta_{\text{HB}}\Theta_{\text{HS}}, \\ \chi^2_{\text{tot}} &= \chi^2_{\text{mass}} + \chi^2_{95} + \chi^2_{\text{EW}} + \chi^2_{\kappa} + \chi^2_{B}. \end{aligned} \tag{30}$$

The total χ^2_{tot} includes only genuine likelihood contributions from the experimental observables, whereas the factors Θ_{PD}, Θ_{unit}, Θ_{HB}, and Θ_{HS} serve as acceptance criteria that restrict the likelihood support to theoretically and phenomenologically viable regions of parameter space.

The individual χ^2 and Θ terms entering Eq. (30) are defined below.

- $\chi^2_{\text{mass}} = \left(\dfrac{m_h - 125.18\ \text{GeV}}{1\ \text{GeV}}\right)^2 + \left(\dfrac{m_H - 95.4\ \text{GeV}}{1\ \text{GeV}}\right)^2$. Here, m_h and m_H denote the theoretically predicted masses of the two CP-even Higgs states, and the total uncertainties, including both theoretical and experimental contributions, are each set to 1 GeV.

- Θ_{HB} implements the direct-search constraints from `HiggsBounds-5.10.0` [161–165]. We define $\Theta_{\text{HB}} = 1$ for parameter points that pass the HiggsBounds exclusion test and $\Theta_{\text{HB}} = 0$ otherwise. In this way, the direct-search constraints act as a veto on the parameter space rather than as a compensating contribution to the global χ^2.

- Θ_{HS} encodes the consistency requirement from `HiggsSignals-2.6.2` [161, 166–168]. To avoid double counting Higgs signal-strength information with the explicit χ^2_{κ} term defined below, we do not include the `HiggsSignals` output as an additive likelihood contribution to χ^2_{tot}. Instead, we require the sample to satisfy $\chi^2(\text{GM}) < \chi^2(\text{SM})$, where $\chi^2(\text{SM}) \approx 152.5$ denotes the SM reference value returned by `HiggsSignals` for the 125 GeV Higgs rate measurements in our setup. Accordingly, we set $\Theta_{\text{HS}} = 1$ when this condition is satisfied and $\Theta_{\text{HS}} = 0$ otherwise.

- $\chi^2_{95} = \left(\dfrac{\mu_{\gamma\gamma} - 0.24}{0.09}\right)^2 + \left(\dfrac{\mu_{\tau\tau} - 1.2}{0.5}\right)^2$ denotes the two excesses at 95 GeV, where $\mu_{\gamma\gamma}$ and $\mu_{\tau\tau}$ are the theoretical predictions including loop corrections.

- The contribution χ^2_{EW} encodes constraints from electroweak precision measurements in terms of the oblique parameters S, T, and U, which capture the one-loop contributions of the additional scalar states to gauge-boson self-energies and neutral-current processes [169, 170]. In this work, χ^2_{EW} is implemented using a multivariate Gaussian form

$$\chi^2_{\text{EW}} = \Delta\vec{O}^T_{\text{EW}}\rho^{-1}_{\text{EW}}\Delta\vec{O}_{\text{EW}}, \tag{31}$$

where

$$\Delta\vec{O}^T_{\text{EW}} = \left(\frac{S + 0.04}{0.10}, \frac{T - 0.01}{0.12}, \frac{U - 0.05}{0.09}\right) \tag{32}$$

and ρ_{EW} denotes the correlation matrix, defined as

$$\rho_{\text{EW}} = \begin{pmatrix} 1 & 0.93 & -0.70 \\ 0.93 & 1 & -0.87 \\ -0.70 & -0.87 & 1 \end{pmatrix}. \tag{33}$$

In addition, the ρ parameter, which characterizes possible new sources of $SU(2)$ breaking beyond the SM Higgs doublet, is constrained to be

$$\rho = 1.00031 \pm 0.00019. \tag{34}$$

In the custodial-symmetric GM setup, $\rho_{\rm tree} = 1$ holds by construction, and any residual deviation arises only at the loop level.

- The contribution χ^2_κ encodes the constraints on the Higgs coupling modifiers through a two-dimensional Gaussian likelihood in the (κ_V, κ_F) plane and is defined as

$$\chi^2_\kappa = \Delta\vec{\kappa}^T\, V^{-1}\, \Delta\vec{\kappa}, \tag{35}$$

where

$$\Delta\vec{\kappa} = \begin{pmatrix} \kappa_V - \hat{\kappa}_V \\ \kappa_F - \hat{\kappa}_F \end{pmatrix}, \tag{36}$$

and V denotes the corresponding covariance matrix

$$V = \begin{pmatrix} \sigma_V^2 & 0.39\sigma_V\sigma_F \\ 0.39\sigma_V\sigma_F & \sigma_F^2 \end{pmatrix}. \tag{37}$$

In our analysis, we use the ATLAS combined fit results shown in Fig. 4 of Ref. [171], namely, $\hat{\kappa}_V = 1.035 \pm 0.031$ and $\hat{\kappa}_F = 0.95 \pm 0.05$, with a correlation coefficient of 0.39.

- $\chi^2_B = \left(\dfrac{\mathcal{B}(B_s \to \mu^+\mu^-) - 3.1\times10^{-9}}{1.3\times10^{-9}}\right)^2 + \left(\dfrac{\mathcal{B}(B \to X_s\gamma) - 3.43\times10^{-4}}{0.44\times10^{-4}}\right)^2$ accounts for constraints from rare B-meson decays, which are highly suppressed in the SM and therefore provide sensitive probes of physics beyond the SM, particularly extended Higgs sectors [172].

In addition to the experimental limits discussed above, theoretical considerations further constrain the parameter space through the Heaviside step functions $\Theta_{\rm unit}$ and $\Theta_{\rm PD}$ in Eq. (30). These functions act as strict vetoes, restricting the likelihood support to theoretically consistent regions of parameter space, where $\Theta(x)$ equals one for $x \geq 0$ and zero otherwise.

$\Theta_{\rm unit}$ enforces perturbative unitarity in scalar $2 \to 2$ scattering by requiring the zeroth partial-wave amplitudes to satisfy $|{\rm Re}\, a_0| < \dfrac{1}{2}$ (equivalently $|a_0| < 1$). In the GM model, this requirement translates into bounds on linear combinations of quartic couplings [173–175], leading to the conditions

$$\begin{aligned} &\sqrt{(6\lambda_1 - 7\lambda_3 - 11\lambda_2)^2 + 36\lambda_4^2} + |6\lambda_1 + 7\lambda_3 + 11\lambda_2| < 4\pi, \\ &\sqrt{(2\lambda_1 + \lambda_3 - 2\lambda_2)^2 + \lambda_5^2} + |2\lambda_1 - \lambda_3 + 2\lambda_2| < 4\pi, \\ &|2\lambda_3 + \lambda_2| < \pi, \\ &|\lambda_4 + \lambda_5| < 2\pi. \end{aligned} \tag{38}$$

Therefore, $\Theta_{\rm unit} = 1$ if all conditions in Eq. (38) are satisfied simultaneously.

The positive-definiteness requirement is imposed to ensure the stability of the electroweak vacuum, so that the scalar potential remains bounded from below for large field values. Quantum corrections can significantly modify the shape of the scalar potential, potentially leading to violations of the tree-level bounded-from-below (BFB) conditions [173]. Such effects may induce deeper vacua at large field values or render the potential unbounded, implying that the electroweak vacuum preserving custodial symmetry is not the true ground state. This situation is reminiscent of the metastability of the SM electroweak vacuum for a 125 GeV Higgs boson.

To address this issue, we impose the positive-definiteness constraints [148] to guarantee the stability of the custodial vacuum by requiring the positivity of certain subdeterminants of the quartic-coupling matrices in the one-loop RG-improved potential. For simplicity, the one-loop RG-improved scalar potential is parameterized by the dimensionless couplings λ, $\rho_{1,2,\cdots,5}$, and $\sigma_{1,2,3,4}$ of the most general $SU(3)_C \times SU(2)_L \times U(1)_Y$-invariant GM model.[1)] In the custodial-symmetric limit, these couplings map onto the standard GM quartics $\lambda_{1,2,\cdots,5}$ as

$$\begin{aligned} &\lambda = 4\lambda_1, \quad \rho_1 = 4\lambda_2 + 6\lambda_3, \quad \rho_2 = -4\lambda_3, \\ &\rho_3 = 2(\lambda_2 + \lambda_3), \quad \rho_4 = 4\lambda_2, \quad \rho_5 = 4\lambda_3, \\ &\sigma_1 = 4\lambda_4 - \lambda_5, \quad \sigma_2 = 2\lambda_5, \quad \sigma_3 = 2\lambda_4, \\ &\sigma_4 = \sqrt{2}\lambda_5. \end{aligned} \tag{39}$$

With these definitions, and when ρ_5 and σ_4 are small, the positive-definiteness constraints reduce to requiring that all leading principal minors of $\mathcal{V}$ be strictly positive,

$$\det \mathcal{V}_n > 0 \qquad (n = 1, 2, \cdots, 5), \tag{40}$$

1) Dimensional parameters are eliminated via the minimization conditions for the VEVs and thus do not affect the large-field analysis relevant to positive definiteness.

where $\mathcal{V}$ is defined as

$$\mathcal{V} = \begin{pmatrix} \frac{1}{4}\lambda & \frac{1}{8}(2\sigma_1+\sigma_2) & \frac{1}{4}\sigma_1 & \frac{1}{2}\sigma_3 & \frac{1}{4}\sigma_3 \\ \frac{1}{8}(2\sigma_1+\sigma_2) & \frac{1}{2}(2\rho_1+\rho_2) & \frac{3}{2}\rho_2 & \rho_4 & \frac{1}{2}\rho_4 \\ \frac{1}{4}\sigma_1 & \frac{3}{2}\rho_2 & \rho_1+\rho_2 & \rho_4 & \frac{1}{2}\rho_4 \\ \frac{1}{4}\sigma_3 & \rho_4 & \rho_4 & 2\rho_3 & \rho_3 \\ \frac{1}{2}\sigma_3 & \frac{1}{2}\rho_4 & \frac{1}{2}\rho_4 & \rho_3 & \frac{1}{2}\rho_3 \end{pmatrix}, \tag{41}$$

and $\mathcal{V}_n$ denotes the $n\times n$ upper-left submatrix of $\mathcal{V}$. Therefore, $\Theta_{\rm PD}$ in Eq. (30) is defined as

$$\Theta_{\rm PD} = \prod_n \Theta(\det \mathcal{V}_n). \tag{42}$$

In practice, the full matrix is used in numerical calculations, whereas the analytic form shown here corresponds to the simplified limit.

It should be noted that the coupling parameters (such as λ, $\rho_{1,2,\cdots,5}$, and $\sigma_{1,2,3,4}$) must be replaced by their renormalization-group-evolved values in regions of large field values. These evolved parameters can then be used to determine the vacuum structure of the GM model. We utilize the iterative method described in [148] to assess whether the parameter space that adequately explains the observed excess signals satisfies the positive-definiteness constraints. The gauge coupling values at the EW scale used in this study are taken from [176]. To ensure that the vacuum preserves custodial symmetry, the boundary conditions for the scalar quartic couplings at the EW scale, which are crucial for the RGEs, are chosen in accordance with Eq. (39). To determine the scale dependence of the quartic couplings within the one-loop RG-improved tree-level scalar potential, it is essential to evolve the input parameters to an arbitrary scale, especially in regions of large field values, using the appropriate beta functions. In our detailed numerical analysis, to establish the positive-definiteness constraints, we evolve the relevant quartic couplings and dimensionful mass parameters from the EW scale ($M_Z = 91.2\,\text{GeV}$) up to the Planck scale ($M_{\rm Planck} \approx 1.12\times10^{19}$ GeV) or to the lowest Landau pole scale, at which any of the quartic couplings diverge.

The tree-level BFB and RG-improved positive-definiteness conditions are not pointwise nested: the former tests the custodial-symmetric quartic potential at the electroweak scale, whereas the latter tracks the general gauge-invariant potential under one-loop evolution to the Planck scale or the first Landau pole. As shown in Refs. [145, 148], the positive-definiteness condition both excludes some regions allowed by BFB and admits some previously excluded regions, yielding a net expansion of the viable parameter space for the 95 GeV excesses.

To ensure a numerically reliable assessment of the GM model's ability to simultaneously explain the two observed excesses, we conducted an extensive exploration of the parameter space using a combination of random scans, Markov Chain Monte Carlo (MCMC) techniques, and MultiNest sampling. These complementary methods provide both broad global coverage and efficient identification of phenomenologically relevant regions with higher likelihood. The final profile-likelihood sample contains $O(10^8)$ retained points after all selections. Convergence was confirmed by verifying the stability of the profile likelihood (PL) under additional sampling.

V. NUMERICAL RESULTS

In this section, we present detailed results from our sampling. For clarity, we exclude all samples that fail the `HiggsBounds` or `HiggsSignals` consistency requirements, the positive-definiteness requirement, or the perturbative unitarity constraints. Thus, all samples shown in the figures satisfy $\Theta_{\rm HB} = 1$, $\Theta_{\rm HS} = 1$, $\Theta_{\rm PD} = 1$, and $\Theta_{\rm unit} = 1$.

A. Fit results and benchmarks

Figure 1 shows the profile likelihood in the $(\mu_{\gamma\gamma}, \mu_{\tau\tau})$ plane for the 95 GeV scalar after applying the constraints of Sec. IV. The preferred region lies near $\mu_{\gamma\gamma} \sim 0.25$ and $\mu_{\tau\tau} \sim 0.47$: the diphoton excess is accommodated near its central value, whereas the ditau excess is only partially reproduced and remains within the experimental 2σ contour.

Compared with Ref. [144], where the tree-level BFB analysis mainly populates the region $\mu_{\tau\tau} \lesssim 0.1$, the RG-

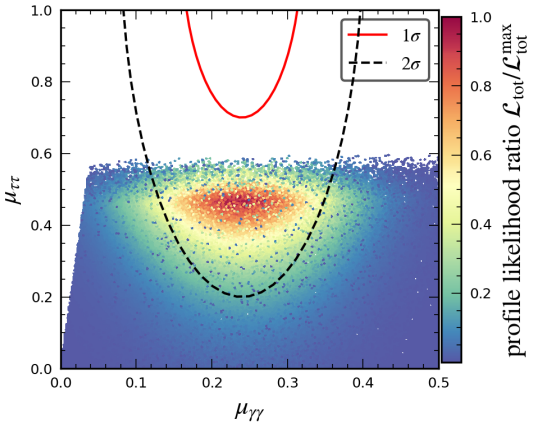


Fig. 1. (color online) Profile likelihood map in the $(\mu_{\gamma\gamma},\mu_{\tau\tau})$ plane. The solid and dashed curves show the experimental 1σ and 2σ contours derived from χ^2_{95}.

improved treatment yields a characteristic ditau signal strength larger by a factor of approximately four to five. Because the scans and likelihoods differ, this should be regarded as a phenomenological cross-check rather than an isolated measure of the vacuum-stability effect.

The inability to fully accommodate the di-tau excess follows from the 125 GeV Higgs-coupling constraints: $\mu_{\tau\tau}$ cannot be increased independently of (κ_F,κ_V), which depend on the common mixing angles α and θ_H, as shown in Eqs. (24) and (22). Figure 2 (left) shows the resulting narrow (κ_F,κ_V) band; $\mathcal{L}_\kappa$ alone favors $\mu_{\tau\tau}\sim 0.4$ (middle), whereas the remaining likelihoods prefer larger values (right). Increasing $|\kappa_F^H|$ also enhances gluon-fusion production and direct-search sensitivity. These competing effects place the combined optimum near the preferred region in Fig. 1 and prevent the fit from approaching the CMS central value.

To highlight the characteristic features of this surviving region, we present three benchmark points in Table 1. `BP1` features a relatively large triplet admixture, with $\sin\theta_H = 0.131$ and $\alpha = -0.808$. This leads to a significant suppression of the SM-like Higgs coupling κ_F. Consequently, the 95 GeV scalar attains a sizable $\mu_{\tau\tau} = 0.742$ and the highest diphoton rate among the three points, $\mu_{\gamma\gamma} = 0.290$, resulting in the smallest χ^2_{95}. However, it does not satisfy the `HiggsSignals` constraints. `BP2` represents the opposite limit, with a very small triplet VEV, $\sin\theta_H = 0.029$. The 125 GeV Higgs is therefore more SM-like. The reduced mixing suppresses the $\tau\tau$ signal strength to $\mu_{\tau\tau} = 0.525$, while the diphoton rate, $\mu_{\gamma\gamma} = 0.237$, is maintained mainly by charged-scalar loop effects. This benchmark satisfies both `HiggsSignals` and `HiggsBounds`. Compared with `BP1`, `BP3` provides a better solution, with $\sin\theta_H = 0.125$ and $\alpha = -1.040$, for which $\kappa_V^h = 0.984$ is remarkably close to the experimental value. This point achieves a balanced configuration, $\mu_{\tau\tau} = 0.545$ and $\mu_{\gamma\gamma} = 0.245$, while remaining consistent with all theoretical and experimental constraints. It exemplifies the thin, correlated region identified in Fig. 2, where the 95 GeV excesses can be accommodated without significantly perturbing the 125 GeV Higgs couplings.

B. Parameter space and phenomenology

Figure 3 displays the PL projected onto the eight GM model parameter planes. A clear pattern emerges: whereas the quartic couplings λ_2, λ_3, λ_4, and λ_5 span relatively broad ranges, the physically relevant mixing parameters are tightly constrained. In the two λ_i panels, no pro-

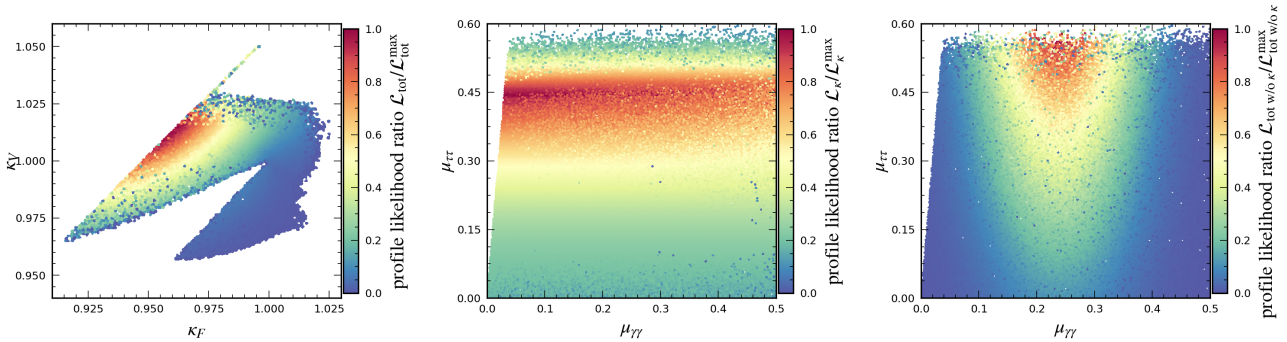


Fig. 2. (color online) Left: The PL map in the (κ_F,κ_V) plane. Middle: The PL $\mathcal{L}_\kappa$ in the $(\mu_{\gamma\gamma},\mu_{\tau\tau})$ plane. Right: The PL $\mathcal{L}_{\rm tot}$, excluding the contribution from $\mathcal{L}_\kappa$, in the $(\mu_{\gamma\gamma},\mu_{\tau\tau})$ plane.

Table 1. Benchmark points in the GM model. The total χ^2 is defined in Eq. (30). A checkmark (√) and a cross (×) indicate whether a given benchmark point passes or fails the corresponding constraint. All dimensional quantities are given in units of GeV.

	BP1	BP2	BP3		BP1	BP2	BP3		BP1	BP2	BP3
λ_2	-0.8211	-0.6069	0.0698	m_H	96.8491	96.68	95.22	$\mu_{\gamma\gamma}$	0.2899	0.2368	0.2445
λ_3	0.8150	0.8336	-0.8805	m_h	124.0331	125.2977	125.0191	$\mu_{\tau\tau}$	0.7423	0.5245	0.5445
λ_4	0.5232	-0.0417	0.4704	m_{H_3}	194.5481	214.3225	222.6281	$\chi^2_{\rm tot}$	19.795	21.220	7.605
λ_5	0.2216	0.8814	-0.0418	m_{H_5}	290.7393	340.3623	311.1941	$\mathcal{B}(H_5^{\pm\pm}\to W^\pm W^\pm)$	0.1757	0.0032	0.1059
α	-0.8075	1.0548	-1.0399	κ_F^h	0.8538	0.9328	0.9330	$\mathcal{B}(H_5^{\pm\pm}\to H_3^\pm W^\pm)$	0.8243	0.9968	0.8941
$\sin\theta_H$	0.1309	0.0287	0.1246	κ_V^h	0.9296	0.9200	0.9836	Unitarity	√	√	√
$M_H^{\rm in}$	96.84	96.6780	95.2205	S	-0.0832	-0.0930	-0.0850	Positive definiteness	√	√	√
$M_h^{\rm in}$	124.0331	125.2977	125.0191	T	-0.0136	-0.0012	-0.0181	`HiggsSignals`	×	√	√
				U	0.0007	0.0003	0.0004	`HiggsBounds`	√	√	√

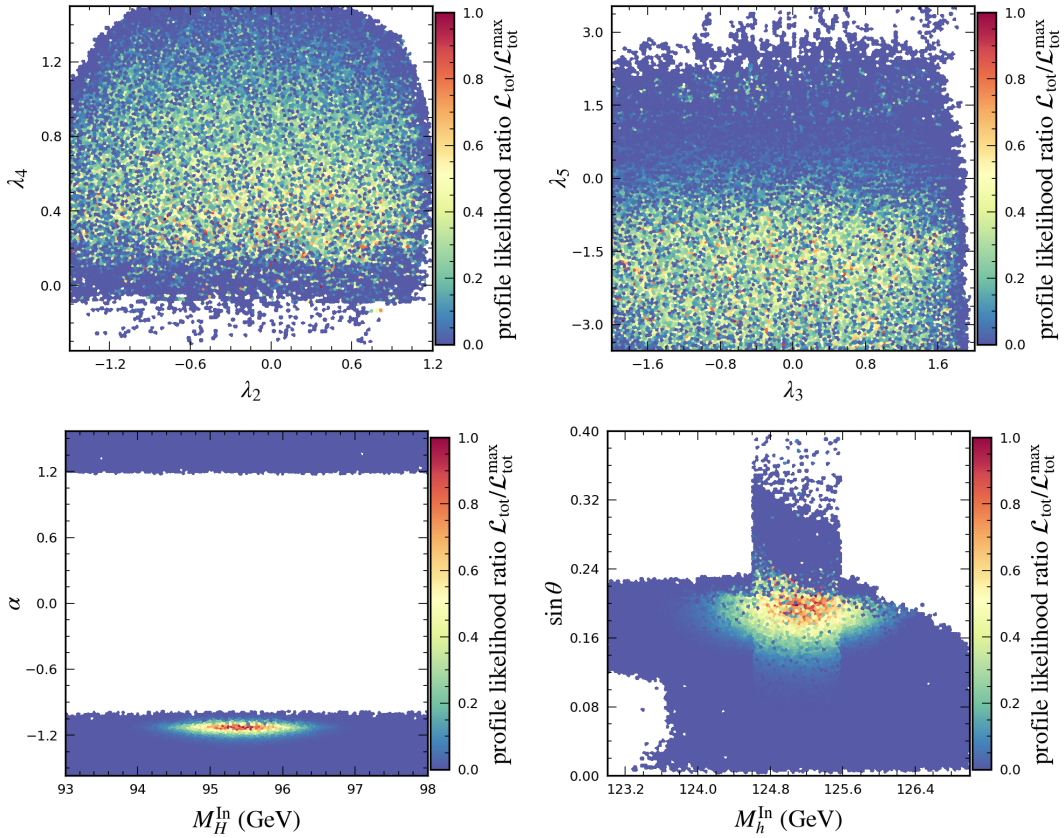


Fig. 3. (color online) Similar to Fig. 1, but shown in the GM model parameter planes.

nounced minima appear, indicating that the quartic interactions are not strongly constrained individually. Instead, these couplings primarily support the scalar mass spectrum and permit viable loop contributions, without requiring finely tuned correlations among themselves. In contrast, the $(M_H^{\rm in},\alpha)$ projection reveals a highly concentrated high-likelihood region centered at $(95\,\text{GeV},-\frac{\pi}{3})$, corresponding directly to the mass of the observed excess. The narrow range of the mixing angle α is consistent with the data, and large portions of the α parameter space are excluded, indicating that doublet–triplet mixing is tightly constrained.

For values of α with identical magnitude, as shown in the benchmark points `BP2` and `BP3`, κ_F remains unchanged, as expected. However, the coupling κ_V associated with positive α is significantly smaller than that for negative α, resulting in a pronounced deviation from the experimental constraints. Moreover, κ_V^H corresponding to positive α is substantially larger than its counterpart for negative α, rendering this scenario incompatible with the additional Higgs-search constraints implemented in the `HiggsBounds` package.

This feature underlies the κ tension observed in Fig. 2: while $\alpha=-\frac{\pi}{4}$ would better explain the excess, the overall fit allows only α near $-\frac{\pi}{3}$. A similar pattern appears in the $(M_h^{\rm in},\sin\theta_H)$ plane. Overall, Fig. 3 demonstrates that the triplet admixture must remain moderate.

The results for the branching ratios of rare B-meson decays and the electroweak precision observables T and S are shown in Fig. 4. These rare B-decay processes are highly suppressed in the SM and are dominated by top-quark and W-boson loops. In the GM model, new charged scalars such as $H_3^\pm$, $H_5^\pm$, and $H_5^{\pm\pm}$ also contribute to these loop diagrams. In our results, the two branching ratios are centered on the experimental central values and exhibit a strong negative correlation. This anti-correlation can be understood at the level of the effective weak Hamiltonian. Both observables are loop-induced flavor-changing neutral-current processes and are therefore sensitive to the charged-scalar sector of the GM model, in particular to the custodial triplet state $H_3^\pm$. The radiative decay $B\to X_s\gamma$ is governed by the electromagnetic dipole operator

$$\mathcal{H}_{\rm eff}\supset-\frac{4G_F}{\sqrt{2}}V_{tb}V_{ts}^*C_7^{\rm eff}O_7,\quad O_7=\frac{e}{16\pi^2}m_b(\bar{s}\sigma^{\mu\nu}P_Rb)F_{\mu\nu}. \tag{43}$$

The branching ratio scales approximately as $\mathcal{B}(B\to X_s\gamma)\propto|C_7^{\rm eff}|^2$ [177, 178]. In contrast, the rare decay $B_s^0\to\mu^+\mu^-$ is governed by

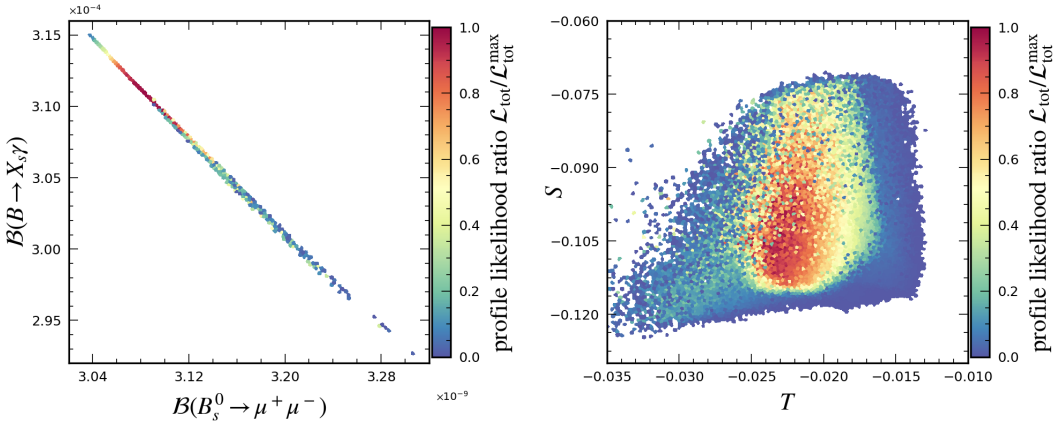


Fig. 4. (color online) Similar to Fig. 1, but shown in the oblique-parameter (T,S) plane and in the branching-ratio plane for the rare B-meson decays $B_s^0 \to \mu^+\mu^-$ and $B \to X_s\gamma$.

$$\mathcal{H}_{\rm eff} \supset -\frac{4G_F}{\sqrt{2}} V_{tb}V_{ts}^*(C_{10}O_{10} + C_S O_S + C_P O_P),$$
$$O_{10} = (\bar{s}\gamma^\mu P_L b)(\bar{\mu}\gamma_\mu\gamma_5\mu), \tag{44}$$

where $O_{S,P}$ denote scalar and pseudoscalar operators. The corresponding branching ratio depends predominantly on $|C_{10}|^2$ in the absence of large scalar contributions [179, 180].

In the GM model, the charged scalars $H_3^\pm$, $H_5^\pm$, and $H_5^{\pm\pm}$ modify both C_7 and C_{10} at the one-loop level. However, the loop functions entering ΔC_7 and ΔC_{10} differ in structure and interfere differently with the SM contributions. For the parameter region relevant to the 95 GeV interpretation, the charged-scalar contribution tends to shift C_7 and C_{10} in opposite effective directions relative to their SM values, leading to the nearly linear anti-correlation observed in Fig. 4.

Turning to the EW oblique observables, the T parameter is often regarded as a sensitive probe of custodial symmetry breaking. In the GM model, custodial symmetry is preserved at tree level, so the main contributions to T arise from mass splittings within the triplet and quintuplet states. For all samples, custodial symmetry remains nearly exact, resulting in $T \approx 0$. However, for larger v_Δ or different values of α, mixing between the light scalar H and the 125 GeV Higgs can shift the masses of certain scalars, inducing mass differences within custodial multiplets and leading to deviations in T.

The S parameter reflects corrections to the Z-boson self-energy and its mixing induced by new-physics states. In the GM model, the S parameter is sensitive to light charged scalars. When the light scalar H has a larger triplet component, such as in the region $\alpha \sim -\pi/3$, loop effects are enhanced, resulting in more significant deviations in S. Conversely, when the 125 GeV Higgs boson is near the alignment limit, such as for $\alpha \sim \pi/3$ and a small triplet vacuum expectation value v_Δ, the scalar sector is dominated by the doublet component, and mixing with the triplet states is suppressed. In this regime, the additional custodial-multiplet scalars either become heavier or couple more weakly to the electroweak gauge bosons. As a result, their loop-induced contributions to the gauge-boson self-energies are reduced, leading to smaller corrections to the oblique parameter S.

Finally, Fig. 5 displays the profiled likelihood projected onto the (M_{H_5}, M_{H_3}) plane. A compressed spectrum is observed between the custodial fiveplet and triplet masses, with $\Delta m(m_{H_5}, m_{H_3}) < O(100\,\text{GeV})$. In particular, the mass hierarchy $M_{H_5} > M_{H_3}$ implies that the doubly charged scalar $H_5^{\pm\pm}$ tends to decay predominantly into $H_3^\pm W^\pm$, rather than through the conventional $W^\pm W^\pm$ mode. As shown in Table 1, the branching ratio $\mathcal{B}(H_5^{\pm\pm} \to W^\pm W^\pm)$ is typically suppressed to below the ten-percent level, and for the benchmark point BP2 it can even reach the per-mille level. This feature has important implications for collider phenomenology.

The right panel of Fig. 5 shows the plane of $m_{H_5^{\pm\pm}}$ versus $\sin\theta_H \sqrt{\mathcal{B}(H_5^{\pm\pm} \to W^\pm W^\pm)}$, together with the published ATLAS limit [181] derived for the simplified topology with dominant $H_5^{\pm\pm} \to W^\pm W^\pm$ decays. We emphasize that this comparison is only indicative. In the cascade-dominated regime relevant to our preferred parameter space, the actual signal topology is controlled by $H_5^{\pm\pm} \to H_3^\pm W^\pm$, and the resulting event kinematics and analysis efficiencies need not coincide with those assumed in the published same-sign diboson search. Therefore, the experimental contour in Fig. 5 should not be interpreted as a strict exclusion bound on the full GM scenario in this region.

Nevertheless, the figure still illustrates an important trend: once the branching ratio into $W^\pm W^\pm$ is strongly suppressed, the direct sensitivity of existing same-sign diboson searches is correspondingly weakened. A dedicated recast of the relevant ATLAS and CMS analyses, explicitly incorporating the cascade topology $H_5^{\pm\pm} \to H_3^\pm W^\pm$, would be required to assess the true collider reach for this

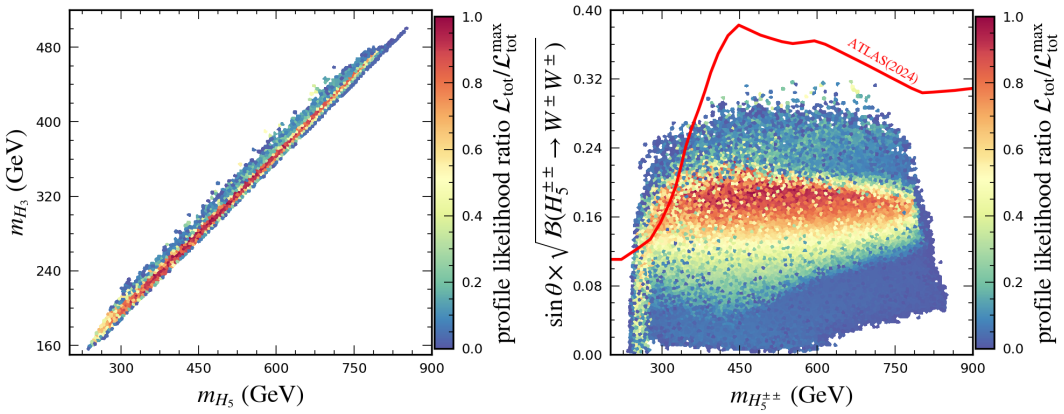


Fig. 5. (color online) Similar to Fig. 1, but showing the (m_{H_5}, m_{H_3}) panel and the $m_{H_5^{\pm\pm}}$ versus $\sin\theta_H\times\sqrt{\mathcal{B}\left(H_5^{\pm\pm}\to W^\pm W^\pm\right)}$ panel. The red line indicates the limit from the ATLAS search [181] for doubly charged $H_5^{\pm\pm}$ in $W^\pm W^\pm$ final states.

part of the parameter space.

Additionally, for the Drell–Yan process, which produces H_5 pairs via γ and Z exchange [182], the production cross section depends only on the gauge coupling and the Higgs mass m_{H_5}, and is independent of v_Δ, as discussed in the experimental searches. In our work, m_{H_5} ranges from several hundred GeV, where the cross section is relatively small, making it difficult for current experimental searches to exclude the surviving parameter space. The process $H_5^{\pm\pm}\to\ell^\pm\ell^\pm$ proceeds via a lepton-number-violating coupling between the triplet χ and the lepton fields, and was studied at LEP [183]. However, as pointed out in [92], this decay channel becomes comparable to the weak gauge boson decay modes only when $v_\Delta\lesssim 10^{-4}$ GeV, making it negligible in the parameter region of interest for our study.

C. Additional checks

As discussed in Sec. 4, our main fit uses the (κ_V,κ_F) likelihood rather than the full `HiggsSignals` output to avoid double counting Higgs signal-strength information. It is nevertheless useful to verify that the preferred region identified in this reduced Higgs-likelihood treatment remains broadly consistent with the more detailed channel-based evaluation provided by `HiggsSignals`. The left panel of Fig. 6 shows the relation between χ^2_κ and $\chi^2_{\rm HS}$, with the color scale indicating the total profile-likelihood ratio.

One can clearly see that parameter points with small χ^2_κ also tend to yield comparatively small $\chi^2_{\rm HS}$ values. This result demonstrates that the simplified (κ_V,κ_F) fit effectively captures the primary Higgs-coupling constraints relevant to our analysis, whereas `HiggsSignals` provides a more comprehensive channel-level evaluation. The spread visible in Fig. 6 indicates that the two approaches are not identical, as expected. In particular, the (κ_V,κ_F) fit is based on a compressed description of the 125 GeV Higgs data and therefore does not retain the full channel-by-channel information, production-mode decomposition, or experimental correlations incorporated in `HiggsSignals`. For this reason, the κ-plane treatment should be regarded as an effective approximation rather

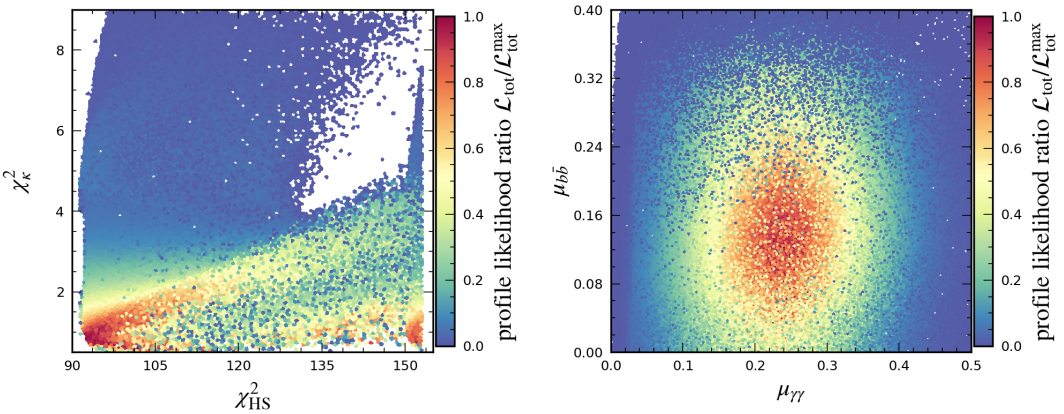


Fig. 6. (color online) Similar to Fig. 1. Left: Relationship between χ^2_κ and $\chi^2_{\rm HS}$, where χ^2_κ is derived from the (κ_V,κ_F)-plane analysis and $\chi^2_{\rm HS}$ is computed using the `HiggsSignals` package. Right: Profile-likelihood distribution projected onto the signal strengths in the $\gamma\gamma$ and $b\bar{b}$ channels.

than a complete replacement for the full Higgs likelihood. In practice, it is also somewhat more conservative than the full channel-based `HiggsSignals` evaluation, since the compressed (κ_V,κ_F) description retains less experimental information and therefore has weaker discriminating power for excluding parameter points. Nevertheless, this comparison tests the robustness of our results. The conclusion that the 95 GeV $\tau\tau$ signal intensity is constrained by 125 GeV Higgs-boson data holds regardless of whether we use the simplified κ-plane method or the more detailed channel-based evaluation.

The right panel of Fig. 6 shows a related feature of the surviving parameter space in the $b\bar{b}$ channel. Although the LEP $b\bar{b}$ excess is not included as an input constraint in our fit, some viable parameter points remain compatible with the corresponding preferred signal-strength range. In the GM model, the $b\bar{b}$ and $\tau\tau$ signal strengths are not independent, since both are controlled by the same underlying singlet–doublet mixing structure and share the common factor $|\kappa_F^H|^2\cdot\Gamma_h^{\rm SM}/\Gamma_H^{\rm tot}$, as discussed in Sec. III. As a result, once the preferred region is selected by the combined $\gamma\gamma$ and $\tau\tau$ fit, the corresponding prediction for $\mu_{b\bar{b}}$ is automatically restricted to a relatively narrow range.

In particular, the best-fit region with $\mu_{\tau\tau}\sim 0.45$ tends to predict a $b\bar{b}$ signal strength close to the central value of the LEP excess. We do not interpret this as a primary target of the present fit, but rather as a correlated outcome of the surviving region selected by the LHC-driven channels. This behavior can be understood qualitatively from the fact that, unlike the $\tau\tau$ excess, the $b\bar{b}$ signal strength does not face the same direct tension with the precision data of the 125 GeV Higgs boson. Consequently, once the Higgs-coupling constraints compress the viable parameter space, the corresponding prediction in the $b\bar{b}$ channel can still remain close to the LEP-preferred range.

Our result should not be viewed as being in conflict with earlier studies, but rather as providing a complementary perspective. Ref. [144] employed a more complete treatment of the Higgs-sector constraints and concluded that the GM model can account for the di-photon excess while remaining compatible with the LEP $b\bar{b}$ excess, but cannot reproduce the large central value of the CMS $\tau\tau$ excess. Ref. [143] further showed that a larger $\tau\tau$ rate can arise either in a tiny single-peak region or, more efficiently, in a twin-peak setup involving multiple nearly degenerate states. In contrast, our analysis focuses on a single light CP-even state and shows that, within this setup, the $\tau\tau$ signal strength can be raised to a moderate level of order 0.5, while larger values are constrained by the 125 GeV Higgs data.

VI. CONCLUSIONS

In this work, we investigated whether a single light CP-even custodial singlet in the Georgi–Machacek model can jointly accommodate the LHC hints near 95 GeV in the $\gamma\gamma$ and $\tau\tau$ channels. The diphoton excess can be accommodated near its central value, whereas $\mu_{\tau\tau}\simeq 0.5$ lies about 1.4σ below the CMS value of 1.2 and is compatible only at the 2σ level.

The one-loop RG-improved positive-definiteness condition reshapes the allowed parameter space relative to the conventional electroweak-scale BFB requirement and yields a net expansion of the phenomenologically viable region, while remaining consistent with perturbative unitarity, electroweak precision data, B-physics observables, direct searches, and Higgs signal-strength measurements.

The preferred region is characterized by a narrow range of the mixing angle, $\alpha\simeq -\pi/3$, a moderate triplet VEV of a few tens of GeV, and a mass hierarchy $m_{H_3}<m_{H_5}$ at the $O(10^2)$ GeV scale. Charged-scalar loops, especially those involving $H_5^{\pm\pm}$, enhance the diphoton rate, allowing it to approach the experimental central value.

These features make the scenario highly testable. Updated $\gamma\gamma$ and $\tau\tau$ searches at the HL-LHC, together with direct probes of the custodial multiplet states, will cover much of the remaining parameter space. Future lepton colliders such as CEPC and FCC-ee will provide decisive tests through precision κ_V measurements.

ACKNOWLEDGMENTS

We thank the reviewers for their constructive comments. We thank Cheng-Wei Chiang and Martin J. White for helpful discussions.

DATA AVAILABILITY STATEMENT

All figures presented in this work were generated using the `Jarvis-PLOT` framework. The complete plotting configuration files used in this study, together with additional result figures not included in the main text, are publicly available at the following webpage:
https://pengxuan-zhu-phys.github.io/Jarvis-Docs/jarvis-plot/pub/gm95excess/

References

[1] G. Aad *et al.* (ATLAS Collaboration), Phys. Lett. B **710**, 49 (2012)
[2] S. Chatrchyan *et al.* (CMS Collaboration), Phys. Lett. B **710**, 26 (2012)
[3] G. Aad *et al.* (ATLAS Collaboration), Phys. Rev. D **101**(1), 012002 (2020)
[4] A. Hayrapetyan *et al.* (CMS Collaboration), Phys. Lett. B

860, 139067 (2025)
[5] A. M. Sirunyan *et al*. (CMS Collaboration), Phys. Lett. B **793**, 320 (2019)
[6] G. Aad *et al*. (ATLAS Collaboration), JHEP **01**, 053 (2025)
[7] T. Biekötter, S. Heinemeyer, and G. Weiglein, Phys. Rev. D **109**(3), 035005 (2024)
[8] A. Tumasyan *et al*. (CMS Collaboration), JHEP **07**, 073 (2023)
[9] R. Barate *et al*. (LEP Working Group for Higgs boson searches, ALEPH, DELPHI, L3, OPAL Collaboration), Phys. Lett. B **565**, 61 (2003)
[10] S. Heinemeyer, Int. J. Mod. Phys. A **33**(31), 1844006 (2018)
[11] S. Heinemeyer and T. Stefaniak, PoS **CHARGED2018**, 016 (2019)
[12] A. Kundu, S. Maharana, and P. Mondal, Nucl. Phys. B **955**, 115057 (2020)
[13] S. Bhattacharya, G. Coloretti, A. Crivellin *et al*., arXiv: 2306.17209
[14] L. Liu, H. Qiao, K. Wang *et al*., Chin. Phys. C **43**(2), 023104 (2019)
[15] K. Wang and J. Zhu, Chin. Phys. C **48**(7), 073105 (2024)
[16] D. Liu, J. Liu, C. E. M. Wagner *et al*., JHEP **06**, 150 (2018)
[17] J. A. Aguilar-Saavedra and F. R. Joaquim, Eur. Phys. J. C **80**(5), 403 (2020)
[18] J. A. Aguilar-Saavedra, H. B. Camara, F. R. Joaquim *et al*., Phys. Rev. D **108**(7), 075020 (2023)
[19] Z. f. Ge, F. Y. Niu, and J. L. Yang, Eur. Phys. J. C **84**(5), 548 (2024)
[20] S. Baek, P. Ko, Y. Omura *et al*., Eur. Phys. J. C **85**(8), 908 (2025)
[21] P. S. B. Dev, R. N. Mohapatra, and Y. Zhang, Phys. Lett. B **849**, 138481 (2024)
[22] S. Ashanujjaman, S. Banik, G. Coloretti *et al*., Phys. Rev. D **108**(9), L091704 (2023)
[23] P. Escribano, V. M. Lozano, and A. Vicente, Phys. Rev. D **108**(11), 115001 (2023)
[24] D. Borah, S. Mahapatra, P. K. Paul *et al*., Phys. Rev. D **109**(5), 055021 (2024)
[25] A. Ahriche, M. L. Bellilet, M. O. Khojali *et al*., Phys. Rev. D **110**(1), 015025 (2024)
[26] F. Richard, arXiv: 1712.06410
[27] D. Sachdeva and S. Sadhukhan, Phys. Rev. D **101**(5), 055045 (2020)
[28] G. Abbas and N. Singh, arXiv: 2412.08523
[29] Z. Li, N. Liu and B. Zhu, arXiv: 2504.21273
[30] S. Yaser Ayazi, M. Hosseini, S. Paktinat Mehdiabadi *et al*., Phys. Rev. D **110**(5), 055004 (2024)
[31] P. J. Fox and N. Weiner, JHEP **08**, 025 (2018)
[32] U. Haisch and A. Malinauskas, JHEP **03**, 135 (2018)
[33] R. Benbrik, M. Boukidi, S. Moretti *et al*., Phys. Lett. B **832**, 137245 (2022)
[34] R. Benbrik, M. Boukidi and B. Manaut, Nucl. Phys. B **1005**, 116593 (2024)
[35] D. Azevedo, T. Biekötter, and P. M. Ferreira, JHEP **11**, 017 (2023)
[36] A. Belyaev, R. Benbrik, M. Boukidi *et al*., JHEP **05**, 209 (2024)
[37] J. Dutta, J. Lahiri, C. Li *et al*., Eur. Phys. J. C **84**(9), 926 (2024)
[38] G. Coloretti, A. Crivellin, and B. Mellado, Phys. Rev. D **110**(7), 073001 (2024)
[39] R. Benbrik, M. Boukidi, and S. Moretti, Phys. Rev. D **110**(11), 115030 (2024)
[40] A. Khanna, S. Moretti, and A. Sarkar, *Explaining 95 GeV Anomalies in the 2-Higgs Doublet Model Type-I*, arXiv: 2409.02587
[41] B. Ait-Ouazghour, M. Chabab, and K. Goure, arXiv: 2410.11140
[42] S. Banik, G. Coloretti, A. Crivellin *et al*., Phys. Rev. D **111**(7), 075021 (2025)
[43] R. Benbrik, M. Boukidi, K. Kahime *et al*., Phys. Lett. B **868**, 139688 (2025)
[44] A. Khanna, S. Moretti, and A. Sarkar, arXiv: 2509.06017
[45] G. Arcadi, G. Busoni, D. Cabo-Almeida *et al*., Phys. Rev. D **110**(11), 115028 (2024)
[46] J. Gao, X. F. Han, J. Ma *et al*., Phys. Rev. D **110**(11), 115045 (2024)
[47] T. Biekötter, M. Chakraborti, and S. Heinemeyer, Eur. Phys. J. C **80**(1), 2 (2020)
[48] T. Biekötter, M. Chakraborti, and S. Heinemeyer, PoS **CORFU2018**, 015 (2019)
[49] T. Biekötter, M. Chakraborti, and S. Heinemeyer, *The "96 GeV excess" in the N2HDM*, arXiv: 1910.06858
[50] T. Biekötter, M. Chakraborti, and S. Heinemeyer, arXiv: 2002.06904
[51] T. Biekötter, M. Chakraborti, and S. Heinemeyer, Int. J. Mod. Phys. A **36**(22), 2142018 (2021)
[52] T. Biekötter, A. Grohsjean, S. Heinemeyer *et al*., Eur. Phys. J. C **82**(2), 178 (2022)
[53] S. Heinemeyer, C. Li, F. Lika *et al*., Phys. Rev. D **106**(7), 075003 (2022)
[54] T. Biekötter, S. Heinemeyer, and G. Weiglein, JHEP **08**, 201 (2022)
[55] T. Biekötter, arXiv: 2304.11439
[56] H. Xu, Y. Wang, X. F. Han *et al*., arXiv: 2505.03592
[57] P. Bechtle, H. E. Haber, S. Heinemeyer *et al*., Eur. Phys. J. C **77**(2), 67 (2017)
[58] J. Cao, X. Guo, Y. He *et al*., Phys. Rev. D **95**(11), 116001 (2017)
[59] K. Choi, S. H. Im, K. S. Jeong *et al*., Eur. Phys. J. C **79**(11), 956 (2019)
[60] J. Cao, X. Jia, Y. Yue *et al*., Phys. Rev. D **101**(5), 055008 (2020)
[61] W. Li, H. Qiao, and J. Zhu, Chin. Phys. C **47**(12), 123102 (2023)
[62] U. Ellwanger and C. Hugonie, Eur. Phys. J. C **83**(12), 1138 (2023)
[63] J. Cao, X. Jia, J. Lian *et al*., Phys. Rev. D **109**(7), 075001 (2024)
[64] W. Li, H. Qiao, K. Wang *et al*., arXiv: 2312.17599
[65] J. Cao, X. Jia, and J. Lian, Phys. Rev. D **110**(11), 115039 (2024)
[66] U. Ellwanger and C. Hugonie, Eur. Phys. J. C **84**(5), 526 (2024)
[67] U. Ellwanger, C. Hugonie, S. F. King *et al*., Eur. Phys. J. C **84**(8), 788 (2024)
[68] J. Lian, Phys. Rev. D **110**(11), 115018 (2024)
[69] C. X. Liu, Y. Zhou, X. Y. Zheng *et al*., Phys. Rev. D **109**(5), 056001 (2024)
[70] T. Biekötter, S. Heinemeyer, and C. Muñoz, Eur. Phys. J. C **79**(8), 667 (2019)
[71] J. Kalinowski and W. Kotlarski, JHEP **07**, 037 (2024)
[72] W. Kotlarski and J. Kalinowski, PoS **CORFU2023**, 121

(2024)
[73] G. Coloretti, A. Crivellin, S. Bhattacharya *et al.*, Phys. Rev. D **108**(3), 035026 (2023)
[74] T. Biekötter, S. Heinemeyer, and G. Weiglein, Phys. Lett. B **846**, 138217 (2023)
[75] S. Banik, G. Coloretti, A. Crivellin *et al.*, JHEP **01**, 155 (2025)
[76] T. Mondal, S. Moretti, and P. Sanyal, Phys. Lett. B **872**, 140041 (2026)
[77] Y. Dong, M. Ruan, K. Wang *et al.*, arXiv: 2506.21454
[78] P. Janot, JHEP **10**, 223 (2024)
[79] G. Bélanger, J. Dutta, R. M. Godbole *et al.*, JHEP **10**, 058 (2024)
[80] H. Georgi and M. Machacek, Nucl. Phys. B **262**, 463 (1985)
[81] M. S. Chanowitz and M. Golden, Phys. Lett. B **165**, 105 (1985)
[82] J. F. Gunion, R. Vega, and J. Wudka, Phys. Rev. D **42**, 1673 (1990)
[83] J. F. Gunion, R. Vega, and J. Wudka, Phys. Rev. D **43**, 2322 (1991)
[84] J. F. Gunion, H. E. Haber, G. L. Kane *et al.*, Front. Phys. **80**, 1 (2000)
[85] H. E. Haber and H. E. Logan, Phys. Rev. D **62**, 015011 (2000)
[86] S. Godfrey and K. Moats, Phys. Rev. D **81**, 075026 (2010)
[87] H. E. Logan and M. A. Roy, Phys. Rev. D **82**, 115011 (2010)
[88] I. Low, J. Lykken, and G. Shaughnessy, Phys. Rev. D **86**, 093012 (2012)
[89] R. Killick, K. Kumar, and H. E. Logan, Phys. Rev. D **88**, 033015 (2013)
[90] A. Efrati and Y. Nir, arXiv: 1401.0935
[91] C. Degrande, K. Hartling, H. E. Logan *et al.*, Phys. Rev. D **93**(3), 035004 (2016)
[92] C. W. Chiang and K. Yagyu, JHEP **01**, 026 (2013)
[93] S. Kanemura, M. Kikuchi, and K. Yagyu, Phys. Rev. D **88**, 015020 (2013)
[94] C. Englert, E. Re, and M. Spannowsky, Phys. Rev. D **87**(9), 095014 (2013)
[95] C. Englert, E. Re, and M. Spannowsky, Phys. Rev. D **88**, 035024 (2013)
[96] S. I. Godunov, M. I. Vysotsky, and E. V. Zhemchugov, J. Exp. Theor. Phys. **120**(3), 369 (2015)
[97] C. W. Chiang and K. Tsumura, JHEP **04**, 113 (2015)
[98] C. W. Chiang, A. L. Kuo, and T. Yamada, JHEP **01**, 120 (2016)
[99] Y. Yu, Y. P. Bi, and J. F. Shen, Phys. Lett. B **759**, 513 (2016)
[100] J. Cao and Y. B. Liu, Mod. Phys. Lett. A **31**(32), 1650182 (2016)
[101] J. Chang, C. R. Chen, and C. W. Chiang, JHEP **03**, 137 (2017)
[102] Y. Zhang, H. Sun, X. Luo *et al.*, Phys. Rev. D **95**(11), 115022 (2017)
[103] B. Li, Z. L. Han, and Y. Liao, JHEP **02**, 007 (2018)
[104] H. Sun, X. Luo, W. Wei *et al.*, Phys. Rev. D **96**(9), 095003 (2017)
[105] G. Azuelos, H. Sun, and K. Wang, Phys. Rev. D **97**(11), 116005 (2018)
[106] J. Cao, Y. Q. Li, and Y. B. Liu, Int. J. Mod. Phys. A **33**(11), 1841003 (2018)
[107] Q. Yang, R. Y. Zhang, W. G. Ma *et al.*, Phys. Rev. D **98**(5), 055034 (2018)
[108] N. Ghosh, S. Ghosh, and I. Saha, Phys. Rev. D **101**(1), 015029 (2020)
[109] A. Ismail, H. E. Logan, and Y. Wu, arXiv: 2003.02272
[110] J. W. Zhu, R. Y. Zhang, W. G. Ma *et al.*, J. Phys. G **47**(12), 125005 (2020)
[111] C. Wang, J. Q. Tao, M. A. Shahzad *et al.*, Chin. Phys. C **46**(8), 083107 (2022)
[112] S. Ghosh, Int. J. Mod. Phys. A **39**(32), 2450139 (2024)
[113] C. H. de Lima and H. E. Logan, Phys. Rev. D **106**(11), 115020 (2022)
[114] A. Ahriche, Phys. Rev. D **107**(1), 015006 (2023)
[115] R. Ghosh and B. Mukhopadhyaya, Phys. Rev. D **107**(3), 035031 (2023)
[116] M. Chakraborti, D. Das, N. Ghosh *et al.*, Phys. Rev. D **109**(1), 015016 (2024)
[117] S. Ghosh, LHEP **2024**, 518 (2024)
[118] S. Bhattacharya, R. Ghosh, and B. Mukhopadhyaya, Phys. Rev. D **111**(5), 053012 (2025)
[119] C.-T. Lu, X. Wang, X. Wei *et al.*, JHEP **02**, 149 (2025)
[120] S. Ghosh, arXiv: 2501.1746
[121] S. Ashanujjaman, A. Crivellin, S. P. Maharathy *et al.*, Phys. Rev. D **112**(3), 035040 (2025)
[122] S. Ghosh, *Fermionic decay of light charged pseudoscalar in Georgi Machacek model*, arXiv: 2506.03772
[123] C. W. Chiang, K. Enomoto, and M. Y. Liao, arXiv: 2506.17541
[124] C. W. Chiang, G. Cottin, and O. Eberhardt, Phys. Rev. D **99**(1), 015001 (2019)
[125] A. Falkowski, S. Rychkov, and A. Urbano, JHEP **04**, 073 (2012)
[126] S. Chang, C. A. Newby, N. Raj *et al.*, Phys. Rev. D **86**, 095015 (2012)
[127] C. W. Chiang, A. L. Kuo, and K. Yagyu, JHEP **10**, 072 (2013)
[128] C. W. Chiang and T. Yamada, Phys. Lett. B **735**, 295 (2014)
[129] T. K. Chen, C. W. Chiang, C. T. Huang *et al.*, Phys. Rev. D **106**(5), 055019 (2022)
[130] R. Zhou, W. Cheng, X. Deng *et al.*, JHEP **01**, 216 (2019)
[131] L. Bian, H. K. Guo, Y. Wu *et al.*, Phys. Rev. D **101**(3), 035011 (2020)
[132] C. T. Lu, Y. Wu, and S. Xu, arXiv: 2504.10930
[133] S. L. Chen, A. Dutta Banik, and Z. K. Liu, Nucl. Phys. B **966**, 115394 (2021)
[134] A. Giarnetti, J. Herrero-Garcia, S. Marciano *et al.*, JHEP **05**, 055 (2024)
[135] A. Giarnetti, J. Herrero-García, S. Marciano *et al.*, Eur. Phys. J. C **84**(8), 803 (2024)
[136] X. K. Du, Z. Li, F. Wang *et al.*, Eur. Phys. J. C **83**(2), 139 (2023)
[137] P. Mondal, Phys. Lett. B **833**, 137357 (2022)
[138] T. K. Chen, C. W. Chiang, and K. Yagyu, Phys. Rev. D **106**(5), 055035 (2022)
[139] R. Ghosh, B. Mukhopadhyaya, and U. Sarkar, J. Phys. G **50**(7), 075003 (2023)
[140] S. Blasi, S. De Curtis, and K. Yagyu, Phys. Rev. D **96**(1), 015001 (2017)
[141] B. Keeshan, H. E. Logan, and T. Pilkington, Phys. Rev. D **102**(1), 015001 (2020)
[142] H. Song, X. Wan, and J. H. Yu, Chin. Phys. C **47**(10), 103103 (2023)
[143] A. Ahriche, Phys. Rev. D **110**(3), 035010 (2024)

[144] T. K. Chen, C. W. Chiang, S. Heinemeyer *et al*., Phys. Rev. D **109**(7), 075043 (2024)
[145] X. Du, H. Liu, and Q. Chang, Phys. Rev. D **112**(1), 015019 (2025)
[146] S. Ghosh, *Light Higgs in the Georgi Machacek Model: neutral or charged*?, arXiv: 2501.17457
[147] P. Mondal and S. Samanta, arXiv: 2506.06427
[148] X. Du and F. Wang, Eur. Phys. J. C **86**(1), 40 (2026)
[149] J. R. Andersen *et al*. (LHC Higgs Cross Section Working Group Collaboration), arXiv: 1307.1347
[150] A. Djouadi, Phys. Rept. **457**, 1 (2008)
[151] A. Djouadi, Phys. Rept. **459**, 1 (2008)
[152] K. Hartling, K. Kumar, and H. E. Logan, arXiv: 1412.7387
[153] W. Porod, Comput. Phys. Commun. **153**, 275 (2003)
[154] W. Porod and F. Staub, Comput. Phys. Commun. **183**, 2458 (2012)
[155] F. Staub, Comput. Phys. Commun. **185**, 1773 (2014)
[156] F. Staub, Comput. Phys. Commun. **184**, 1792 (2013)
[157] F. Staub, Comput. Phys. Commun. **182**, 808 (2011)
[158] F. Staub, Comput. Phys. Commun. **181**, 1077 (2010)
[159] F. Staub, arXiv: 0806.0538
[160] E. Guo, P. Jackson, J. M. Yang *et al*., arXiv: 2604.25557
[161] H. Bahl, T. Biekötter, S. Heinemeyer *et al*., Comput. Phys. Commun. **291**, 108803 (2023)
[162] P. Bechtle, O. Brein, S. Heinemeyer *et al*., Comput. Phys. Commun. **181**, 138 (2010)
[163] P. Bechtle, O. Brein, S. Heinemeyer *et al*., Comput. Phys. Commun. **182**, 2605 (2011)
[164] P. Bechtle, O. Brein, S. Heinemeyer *et al*., Eur. Phys. J. C **74**(3), 2693 (2014)
[165] P. Bechtle, D. Dercks, S. Heinemeyer *et al*., Eur. Phys. J. C **80**(12), 1211 (2020)
[166] P. Bechtle, S. Heinemeyer, O. Stal *et al*., Eur. Phys. J. C **74**(2), 2711 (2014)
[167] P. Bechtle, S. Heinemeyer, O. Stal *et al*., JHEP **11**, 039 (2014)
[168] P. Bechtle, S. Heinemeyer, T. Klingl *et al*., Eur. Phys. J. C **81**(2), 145 (2021)
[169] M. E. Peskin and T. Takeuchi, Phys. Rev. Lett. **65**, 964 (1990)
[170] M. E. Peskin and T. Takeuchi, Phys. Rev. D **46**, 381 (1992)
[171] G. Aad *et al*. (ATLAS Collaboration), Nature **607**(7917), 52 (2022)
[172] V. Khachatryan *et al*. (CMS, LHCb Collaboration), Nature **522**, 68 (2015)
[173] K. Hartling, K. Kumar, and H. E. Logan, Phys. Rev. D **90**(1), 015007 (2014)
[174] D. Chowdhury, P. Mondal and S. Samanta, arXiv: 2404.18996
[175] M. Aoki and S. Kanemura, Phys. Rev. D **77**(9), 095009 (2008)
[176] S. Antusch and V. Maurer, JHEP **11**, 115 (2013)
[177] A. J. Buras, arXiv: hep-ph/9806471
[178] M. Misiak *et al*., Phys. Rev. Lett. **114**(22), 221801 (2015)
[179] C. Bobeth, M. Gorbahn, T. Hermann *et al*., Phys. Rev. Lett. **112**, 101801 (2014)
[180] T. Hermann, M. Misiak and M. Steinhauser, JHEP **12**, 097 (2013)
[181] G. Aad *et al*. (ATLAS Collaboration), JHEP **04**, 026 (2024)
[182] G. Aad *et al*. (ATLAS Collaboration), JHEP **06**, 146 (2021)
[183] G. Abbiendi *et al*. (OPAL Collaboration), Phys. Lett. B **526**, 221 (2002)